Available online at www.sciencedirect.com
ScienceDirect
International Journal of Thermal Sciences 45 (2006) 1113–1125
International Journal of Thermal Sciences
www.elsevier.com/locate/ijts

A numerical study on entropy generation and optimization for laminar forced convection in a rectangular curved duct with longitudinal ribs

T.-H. Ko *

Department of Mechanical Engineering, Lunghwa University of Science and Technology, 300, Wan-Shou Rd., Sec. 1, Kueishan, 33306, Taoyuan, Taiwan, ROC

Received 10 January 2006; received in revised form 5 March 2006; accepted 9 March 2006

Available online 27 April 2006

Abstract

The effects of longitudinal ribs on laminar forced convection and entropy generation in a curved rectangular duct are investigated in the present paper by numerical methods. The major concern is to explore the optimal rib number and arrangement of the mounted rib based on the minimal entropy generation principle. The detailed information of local distributions of entropy generation due to frictional and heat transfer irreversibility as well as the overall entropy generation in the whole flow field are analyzed separately. The results show that the flow features in the curved duct, including the secondary flow motion, and the distributions of velocity and temperature, are considerably influenced by the number and arrangement of mounted ribs. Through the comparison of the cases with none to four ribs mounted on duct walls with various arrangements, it is found that a single rib on the heated duct wall is the most effective way to reduce entropy generation, whereas additional ribs can not give further reduction in entropy generation. The rib arrangement is suggested to be used in practical applications so that the irreversibility due to the laminar forced convection in the curved duct would be minimal and the best exergy utilization could be achieved.

Keywords: Entropy generation; Laminar forced convection; Irreversibility; Exergy

1. Introduction

The rectangular curved duct extensively appears in various industrial applications. It usually plays an important role as heat exchange passages for heat exchangers. Because of practical importance, the flow dynamics and heat transfer in rectangular curved ducts have received continuous attention during past several decades [1–9]. From these studies, a common conclusion indicates that the secondary flow motion, which is the most important flow feature in rectangular curved ducts, can effectively enhance heat transfer performance. However, it is also found that the secondary flow motion induces more serious pressure drop in flow fields. Actually, an unavoidable conflict has risen disconcerting to the current heat exchanger designs, i.e. a design parameter adjusted to improve the heat transfer performance inevitably induces the simultaneous increase in pressure loss. Such situation makes the optimal design through the trade-off between the enhancement of heat transfer performance and reduction of pressure loss become a major concern for the design work of modern thermal systems. Although the design of the rectangular curved duct also faces such a challenge, it is found that most of the previous relevant studies were restricted to the analysis based on Thermodynamic First Law from which the optimal analysis for the rectangular curved duct could hardly be carried out.

Recently, optimal designs of thermal systems have been widely proposed from the viewpoint of Thermodynamic Second Law [10–24]. The minimal entropy generation principle has become an important consideration for the heat exchanger design. The optimal design work for rectangular curved ducts based on the minimal entropy generation principle was first reported in recent work of Ko and Ting [19]. In the study, the entropy generation due to laminar forced convection in a curved rectangular duct with constant wall heat flux was investigated. The optimal Dean number and optimal aspect ratio of duct cross-section according to various relevant design parameters for the rectangular curved duct were analyzed based on minimal entropy generation principle. With numerical meth-

* Tel.: +886 2 82093211; fax: +886 2 82091475.
E-mail address: thko@mail.lhu.edu.tw (T.-H. Ko).

1290-0729/$ – see front matter
doi:10.1016/j.ijthermalsci.2006.03.003

Nomenclature

a	width of the cross-sectional area of rectangular curved duct	m	
A	cross-sectional area of duct	m^2	
b	height of the cross-sectional area of rectangular curved duct	m	
Be	Bejan number		
C_{sec}	secondary kinetic energy coefficient		
d_e	hydraulic diameter	m	
De	Dean number, $= Re(d_e/r_c)^{1/2}$		
h	rib height	m	
$\bar{h}$	average heat transfer coefficient in the rectangular curved duct	$W m^{-2} K^{-1}$	
k	thermal conductivity of fluid	$W m^{-1} K^{-1}$	
k_s	thermal conductivity of steel	$W m^{-1} K^{-1}$	
Nu	Nusselt number, $= \bar{h}d_e/k$		
P	pressure	Pa	
P_W	wetted perimeter of duct	m	
q''	wall heat flux	$W m^{-2}$	
q^*	non-dimensional heat flux		
$\dot{Q}$	heat transfer rate	W	
R	gas constant	$J kg^{-1} K^{-1}$	
Re	Reynolds number		
r_c	radius of curvature	m	
S'''_P	volumetric entropy generation rate due to friction	$W m^{-3} K^{-1}$	
S'''_T	volumetric entropy generation rate due to heat transfer	$W m^{-3} K^{-1}$	
S'''_{gen}	total volumetric entropy generation rate	$W m^{-3} K^{-1}$	
S^*_P	non-dimensional entropy generation rate due to friction		
S^*_T	non-dimensional entropy generation rate due to heat transfer		
S^*_{gen}	non-dimensional entropy generation rate		
T	temperature	K	
T_0	temperature at duct entrance	K	
$\overline{V}$	average velocity in duct	$m s^{-1}$	
V	volume of curved duct		
V_1, W_1	velocity components in the duct cross-section	$m s^{-1}$	
μ	molecular viscosity	$kg m^{-1} s^{-1}$	
ρ	density	$kg m^{-3}$	

ods later, Ko [20] investigated the laminar forced convection and entropy generation in a curved rectangular duct with a single longitudinal rib mounted at midway of the heated wall. The mounted rib with proper sizes was found to result in a significant reduction of entropy generation in the flow field. Through the entropy generation analysis and minimal entropy generation principle, the optimal rib size for the rectangular curved duct with different flow conditions were discussed in detail in the paper. However, since in the previous work [20], only the case with single longitudinal rib mounted on the duct wall was considered, the effects of rib numbers and their arrangements are still left unexplored. The present paper is a sequent study concerning the effects of longitudinal ribs on the laminar forced convection and entropy generation in rectangular curved ducts. The major purpose is to investigate the effects of rib numbers and rib arrangements mounted on curved duct wall by numerical methods. Through the analysis of the influences of mounted ribs on entropy generations, the optimal rib number and arrangement for the rectangular curved duct is reported in the paper based on the minimal entropy generation principle.

2. Physical model

Fig. 1 shows the semi-circular curved rectangular duct analyzed in the present paper. The cross-section of the curved duct is square, and its side length is denoted as a. The Reynolds number (Re), Nusselt number (Nu) and Dean number (De) for the current problem are defined as follows:

$$Re = \rho \overline{V} d_e/\mu \tag{1}$$

$$Nu = \bar{h} d_e/k \tag{2}$$

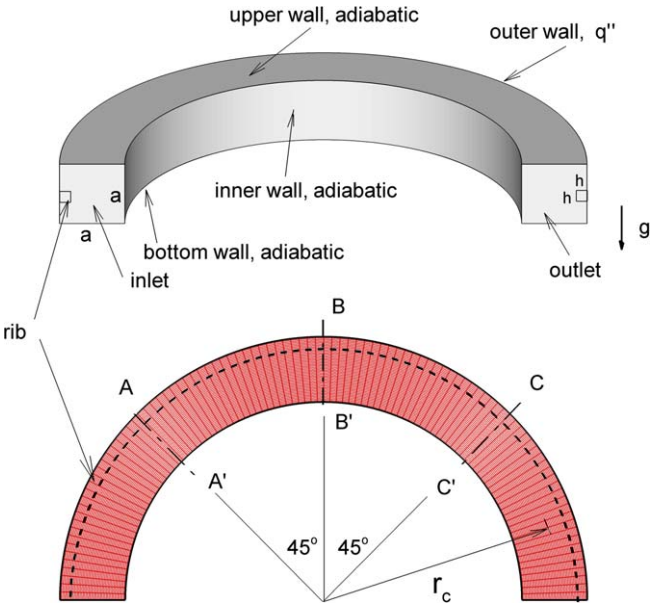

Fig. 1. Rectangular curved duct with rib mounted on the heated (outer) wall.

and

$$De = Re(d_e/r_c)^{1/2} \tag{3}$$

where $\overline{V}$ and $\bar{h}$ are the average velocity and average heat transfer coefficient of the flow in the curved duct; d_e is the characteristic length defined as $4A/P_W$, where A and P_W are the area and wetted perimeter of the square cross-section, respectively; r_c is the curvature radius of the curved duct. Longitudinal steel ribs with square cross-section are mounted on the duct wall. In

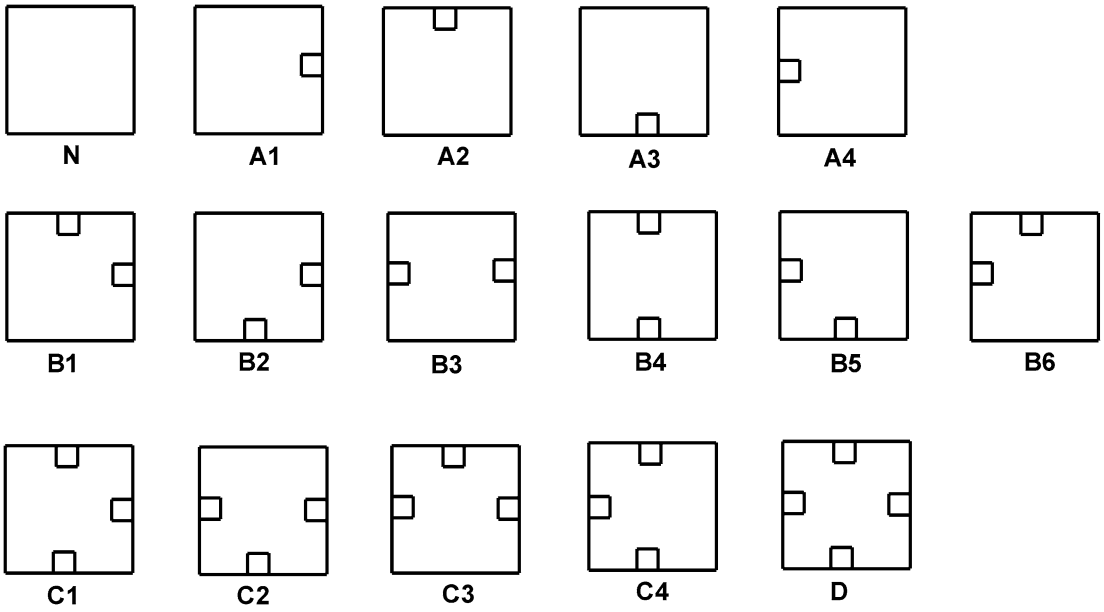

Fig. 2. Various rib arrangements of analyzed cases. Outer wall is at right-hand side, inner wall is at left-hand side.

the present paper, four groups of analyzed cases with rib number from one to four are investigated. In each group, several cases with different rib arrangements are considered. All the analyzed cases are shown in Fig. 2, in which the right-hand side of each cross-section is duct outer wall, and the left-hand side is the duct inner wall. The case without rib denoted by N is also included for comparison. The rib height h is fixed as $1/7d_e$ in all cases since in the previous study of Ko [20] the rib size has been verified to be capable of inducing the minimal entropy generation in the flow field. The density and thermal conductivity of the steel rib are 7900 $\mathrm{kg\,m^{-3}}$ and 200 $\mathrm{W\,m^{-1}\,K^{-1}}$, respectively. Air has been selected as working fluid. Since temperature change in the flow field is very small, the thermophysical properties of molecular viscosity (μ) and thermal conductivity (k) are assumed to be constant as 1.846×10^{-5} $\mathrm{kg\,m^{-1}\,s^{-1}}$ and 0.0263 $\mathrm{W\,m^{-1}\,K^{-1}}$, respectively. The buoyancy force due to gravity has been included in the analysis. The gravity direction is indicated in Fig. 1. The fluid density at duct entrance according to the fluid temperature T_0 is 1.161 $\mathrm{kg\,m^{-3}}$. The non-dimensional wall heat flux, q^*, is defined according to the external wall heat flux, q'', as

$$q^* = q'' d_e / kT_0 \tag{4}$$

Fig. 1 also indicates the positions of the three duct cross-sectional planes: A–A′, B–B′ and C–C′. In the following, some discussion is based on the flow structures on the three planes.

3. Mathematical model and numerical method

3.1. Mathematical model

The present problem is assumed as three-dimensional, laminar and steady. The largest *De* considered in the current paper is 2000. From the discussion in the previous work of Ko and Ting [19], the flows are confirmed as in laminar regime. The conjugated heat transfer phenomena including the heat transfer in fluid flow and conduction in steel ribs are considered simultaneously in the current analysis. The governing equations that apply are: continuity equation, Navier–Stokes equation and energy equation for fluid flow, and the thermal conduction equation for steel ribs. The boundary conditions are, as follows: Uniform axial velocity is set at duct inlet. Zero diffusion flux in the direction perpendicular to the outlet plane of duct exit for all velocity components and T are set to zero at outlet. On all solid walls, including the duct wall and rib wall, non-slip conditions are specified. As shown in Fig. 1, the constant heat flux is specified only on the outer wall, while on other duct walls, the adiabatic condition is assumed. At the interface between fluid and rib surface, the energy balance of convection in fluid flow and conduction in steel rib is applied to represent the conjugate heat transfer process. All of the governing equations and boundary conditions mentioned above have been described in Ref. [19]. Therefore, the details are not repeated here. After the velocity and temperature distributions of the flow field are solved, the volumetric entropy generation due to fluid frictional irreversibility (S'''_P) and heat transfer irreversibility (S'''_T) can be calculated by the following equations [11]:

$$S'''_P = \frac{\mu}{T}\left(\frac{\partial U_i}{\partial x_j} + \frac{\partial U_j}{\partial x_i}\right)\frac{\partial U_i}{\partial x_j} \tag{5}$$

$$S'''_T = \frac{k}{T^2}\left(|\nabla T|\right)^2 \tag{6}$$

and the total volumetric entropy generation can be obtained by

$$S'''_{\mathrm{gen}} = S'''_T + S'''_P \tag{7}$$

Bejan number (*Be*) proposed by Paoletti et al. [25] is a parameter that describes the contribution of heat transfer entropy generation on overall entropy generation, which is defined as

$$Be = S'''_T / S'''_{\mathrm{gen}} \tag{8}$$

The range of Be is from 0 to 1; $Be = 0$ and $Be = 1$ are two limiting cases representing the irreversibility is dominated by fluid friction and heat transfer, respectively.

For evaluation of the entropy generation in whole flow field, the non-dimensional entropy generation rate, S_P^*, S_T^* and S_{gen}^*, in the whole curved duct are defined by

$$S_P^* = \frac{\int_V S_P''' \, \mathrm{d}V}{\dot{Q}/T_0} \tag{9}$$

$$S_T^* = \frac{\int_V S_T''' \, \mathrm{d}V}{\dot{Q}/T_0} \tag{10}$$

and

$$S_{\text{gen}}^* = \frac{\int_V S_{\text{gen}}''' \, \mathrm{d}V}{\dot{Q}/T_0} \tag{11}$$

where V is the volume of the whole computational domain, including the fluid and the steel ribs; $\dot{Q}$ is the heat flow rate into the flow field.

3.2. Numerical method

The above-mentioned equations accompanied with boundary conditions are discretized by a finite volume formulation. The well-known SIMPLE algorithm is adopted as numerical solution procedure. The detailed numerical procedure can be found in [26]. The convergent criteria is set as the relative residual of all variables, including mass, velocity components and temperature less than 10^{-4}. A commercial CFD software CFD RC (ESI US R&D, Inc.) is used for the numerical solution.

4. Results and discussion

The accuracy of numerical solutions has been investigated through the comparison of current numerical results with the experimental data of Chandratilleke [7] and the numerical results by Chandratilleke and Nursubyakto [8] for the forced convective flows in the curved duct with various aspect ratios. From the comparisons, which have been discussed in a previous study of Ko and Ting [19], the accuracy of numerical results has been verified. In addition, the grid independent test has also been carried out in the previous study [19]. For higher resolution of the current problem, the grid number is raised to about 250 000 for ducts with various rib number and arrangements.

In the following, the flow features, including velocity contours, secondary flow motion, temperature distribution, and the detailed distribution of local entropy generation are presented and discussed first. The optimal analysis of cases with various De and q^* based on minimal entropy generation principle is followed.

4.1. Effects of rib number and arrangement on the flow fields

For investigating the effects of rib number and arrangement mounted on the curved duct wall, the flow fields of five selected baseline cases, including the cases without rib (case N), with one rib (case A1), two ribs (case B1), three ribs (case C1) and four ribs (case D), are discussed first. In these cases, q^* and De are fixed as 0.112 and 1000, respectively. The most important flow feature in curved ducts is the secondary flow motion resulting from curvature effects. Fig. 3 shows vector plots on the cross-sectional planes of A–A′, B–B′ and C–C′ for the five cases, respectively, which indicate the developments of secondary flow motion. For the case without rib (case N), two pairs of vortices form on A–A′ plane: one pair is located near the duct outer wall, and the other pair composed of two vortices with long and narrow shape distributes adjacent to the upper and lower walls. As the flow develops to B–B′ and C–C′ planes, the vortices near outer wall gradually become larger and move toward duct central zone slightly, whereas the size and position of the vortices near upper and lower walls remain almost unchanged. The influence of mounted ribs on the secondary flow motion can be clearly detected from the ribbed cases. When comparing with the no-rib case N, the principal pattern of the vortex structure in the one-rib case A1 has no apparent change, but the dual vortices adjacent to the outer wall can be seen to be separated by the rib and become more distinguishable. In the two-rib case B1, the vortex motion is much more complicated. On A–A′ plane, the vortex pair near outer wall remains similar to that of cases N and A1. However, the symmetric vortex pattern in cases N and A is destroyed by the extra rib on top wall. The original long and narrow vortex near top wall is impeded by the rib and separated into two vortices. At sections B–B′ and C–C′, the vortex motion is further more complicated by the rib on top wall. The sizes of the dual vortices adjacent to the outer wall become unequal on B–B′ plane unlike those in previous cases. On plane C–C′, a new vortex pair with vortices of different sizes appear near the rib and distribute in the zone between the dual vortices next to the outer wall. The principal vortex pattern in the three-rib cases C1 is similar to that in case B1, except the long and narrow vortex near the bottom wall is impeded and separated into two vortices by rib bottom, similar to the situation near the top wall. Due to the symmetric configuration in this case, the sizes of vortices between the vortex pair adjacent to the outer wall become the same again. When comparing the four-rib case D with case C1, it is found the vortex systems in the two cases are almost the same, which indicates the rib mounted on the inner wall does not induce significant affects on the secondary motion in the curved duct.

For understanding the development of the strength of secondary motions, the secondary kinetic energy coefficient, C_{sec}, is defined as

$$C_{\text{sec}} = \left(V_1^2 + W_1^2\right)^{1/2} / \overline{V} \tag{12}$$

where V_1 and W_1 are two velocity components in duct cross-section. Since the strength of the secondary flow motion is dependent on the velocity components on the duct cross-sectional plane normal to the axial flow direction, the magnitude of C_{sec} is a quantity to represent the strength of secondary motion. Fig. 4 provides the distribution of C_{sec} on A–A′, B–B′ and C–C′ planes for the five cases, respectively. In the non-rib case N, the larger C_{sec} appears in the region adjacent to the top and lower walls on A–A′ and B–B′ planes, and transfers to the duct central zone with inclination to the outer wall on C–C′ plane.

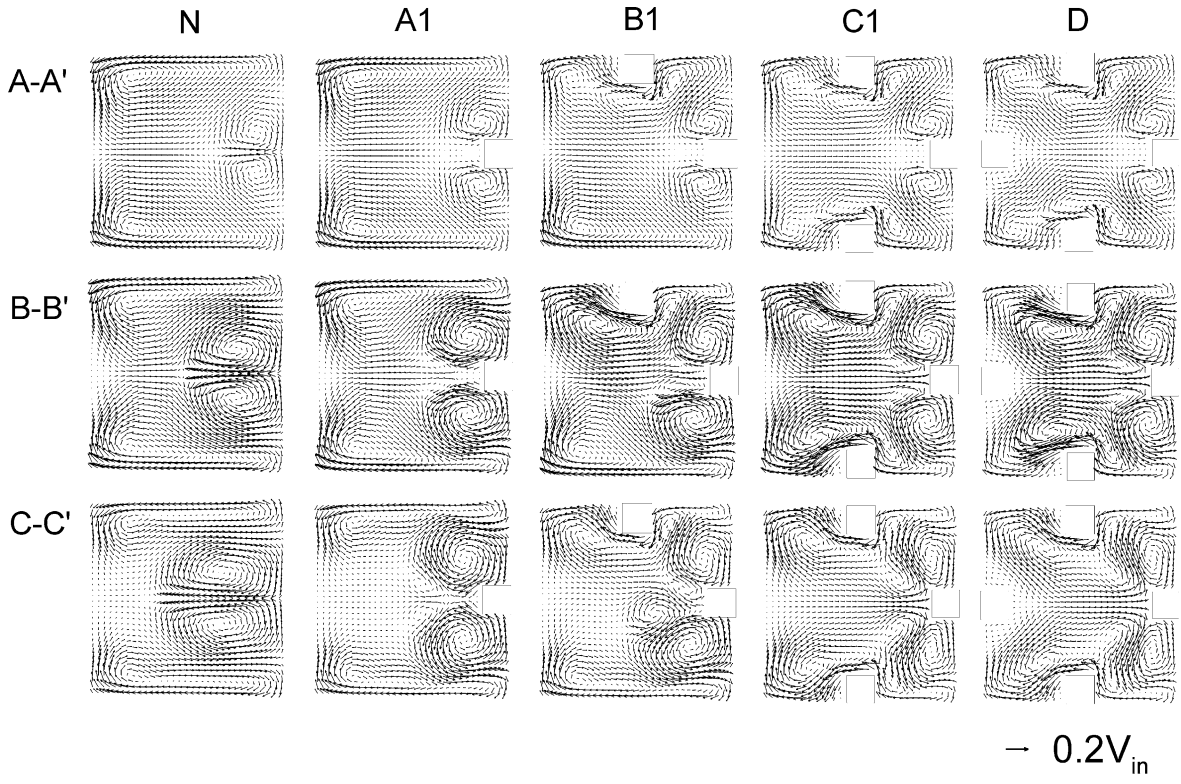

Fig. 3. Flow analysis: secondary flow motions on cross-sectional planes at A–A′, B–B′ and C–C′. (a) No rib, case N; (b) one rib, case A1; (c) two ribs, case B1; (d) three ribs, case C1; (e) four ribs, case D. On each cross-sectional plane, outer wall is at right-hand side, inner wall is at left-hand side.

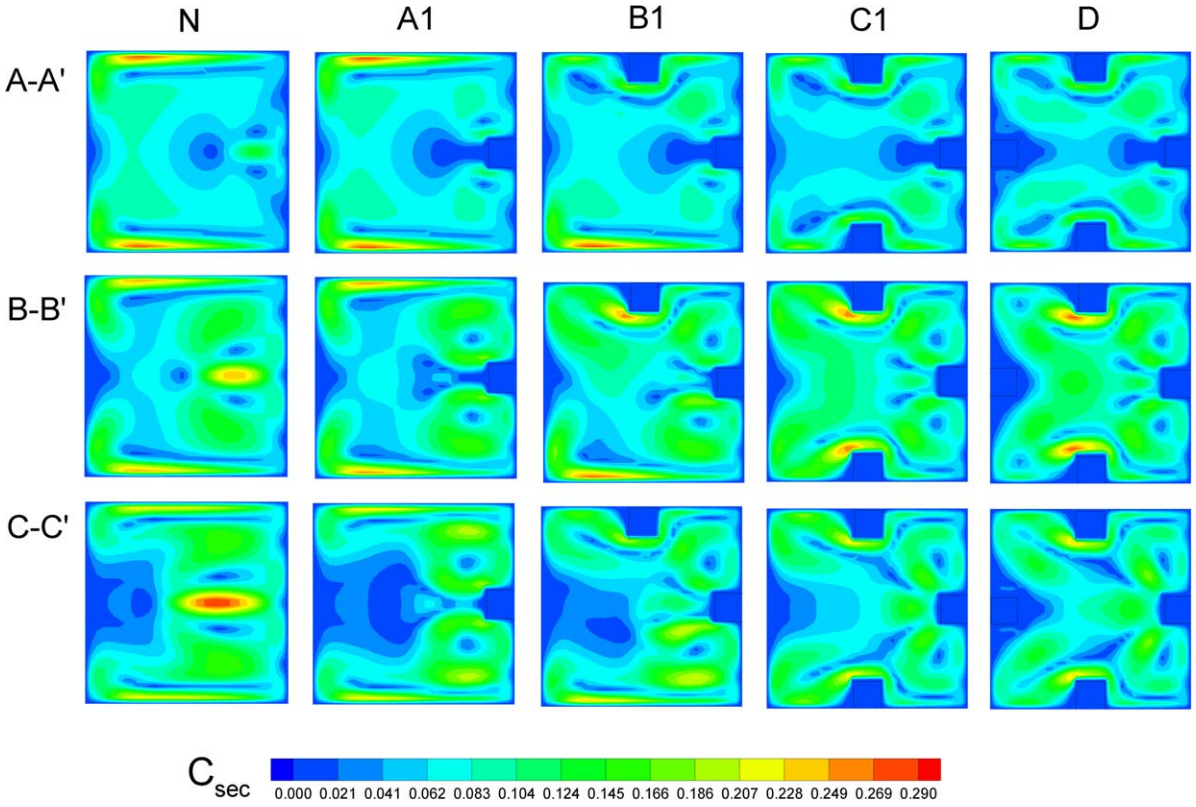

Fig. 4. Distributions of secondary kinetic energy coefficient, C_{sec}, on cross-sectional planes at A–A′, B–B′ and C–C′. (a) No rib, case N; (b) one rib, case A1; (c) two ribs, case B1; (d) three ribs, case C1; (e) four ribs, case D. On each cross-sectional plane, outer wall is at right-hand side, inner wall is at left-hand side.

The magnitudes of largest C_{sec} on A–A′, B–B′ and C–C′ planes are 0.279, 0.253 and 0.281, respectively, which indicates the largest C_{sec} takes place on C–C′ plane in case N. For one-rib case A1, the largest C_{sec} occurs in the narrow region in vicinity of the upper and lower walls on all of the three planes. The value of the largest C_{sec} decreases gradually from A–A′ plane to C–C′ plane, indicating the strength of second flow motion decreases as the flow develops along the duct. In the two-rib case B1, it is seen that the largest C_{sec} on A–A′ plane occurs only in the region near the lower wall, whilst the value of C_{sec} near the top wall is influenced by the rib and becomes smaller than that near the lower wall. On B–B′ plane, the largest C_{sec} occurs in the vicinity of the lower wall, and the value of C_{sec} near the rib corner on the top wall again increases to the value as large as that near the lower wall. But the largest value of C_{sec} on B–B′ plane decreases as smaller than that on A–A′ plane. On C–C′ plane, the largest value of C_{sec} further decreases. The distributions of C_{sec} for cases C1 and D are very similar. The largest C_{sec} occurs on B–B′ plane and distributes in the rib-corner regions near the top and lower walls.

Fig. 5 shows the distribution of constant velocity contours on A–A′, B–B′ and C–C′ planes for the five cases, respectively. For the no-rib case N, it is seen that the curvature of the curved duct makes the flow patterns on inner and outer sides asymmetric on the three cross-sectional planes. On A–A′ plane, the larger-velocity contours form a U-shape. The low-velocity fluid occupies the U-shape concave region near the outer wall, where there is the local region with stronger secondary flow motion on the plane. As the flow develops toward B–B′ and C–C′ planes, the low-velocity region penetrates toward the duct central zone gradually, whilst the higher velocity region transfers toward outer side due to the centrifugal effects. On C–C′ plane, the higher velocity region is separated into two distinct zones, between which is the region occupied by the stronger secondary flow motions. For one-rib case A1, the basic pattern and development of velocity distributions are similar to those in case N. Due to the impediment of rib, the low-velocity region distributing around the rib and the region with stronger secondary flow motion becomes wider than those in case N. Besides, the complex combined effects of centrifugal force and rib impediments make the largest velocity occur on the midway of C–C′ plane. In the two-rib case B1, the velocity distribution becomes asymmetric not only in inner and outer sides but also in upper and lower sides. The existence of the rib on upper wall, accompanied with the centrifugal effects, makes the fluid with higher velocity move toward the outer and lower region. The flow patterns in the three- and four-rib cases C1 and D are very similar. In the two cases, the impediment of ribs makes the higher-velocity fluid concentrate in the duct central region, but still inclined toward outer side due to the influences of centrifugal effects.

Fig. 6 shows the temperature distributions on A–A′, B–B′ and C–C′ planes for the five cases. On all planes for the five cases, it is seen from the figures that the higher temperature zone concentrates in the region adjacent to the outer wall, where the external heat flux is applied. The temperature rise in all

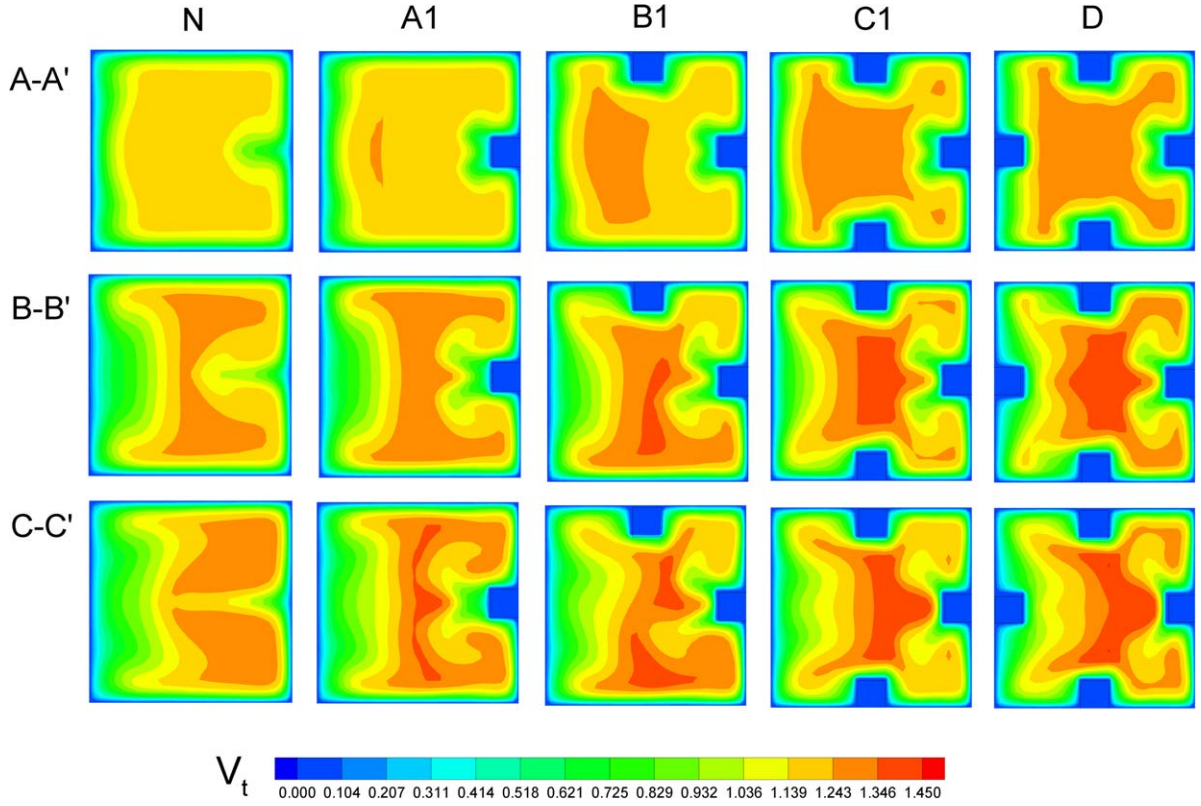

Fig. 5. Flow analysis: velocity contours on cross-sectional planes at A–A′, B–B′ and C–C′. (a) No rib, case N; (b) one rib, case A1; (c) two ribs, case B1; (d) three ribs, case C1; (e) four ribs, case D. On each cross-sectional plane, outer wall is at right-hand side, inner wall is at left-hand side.

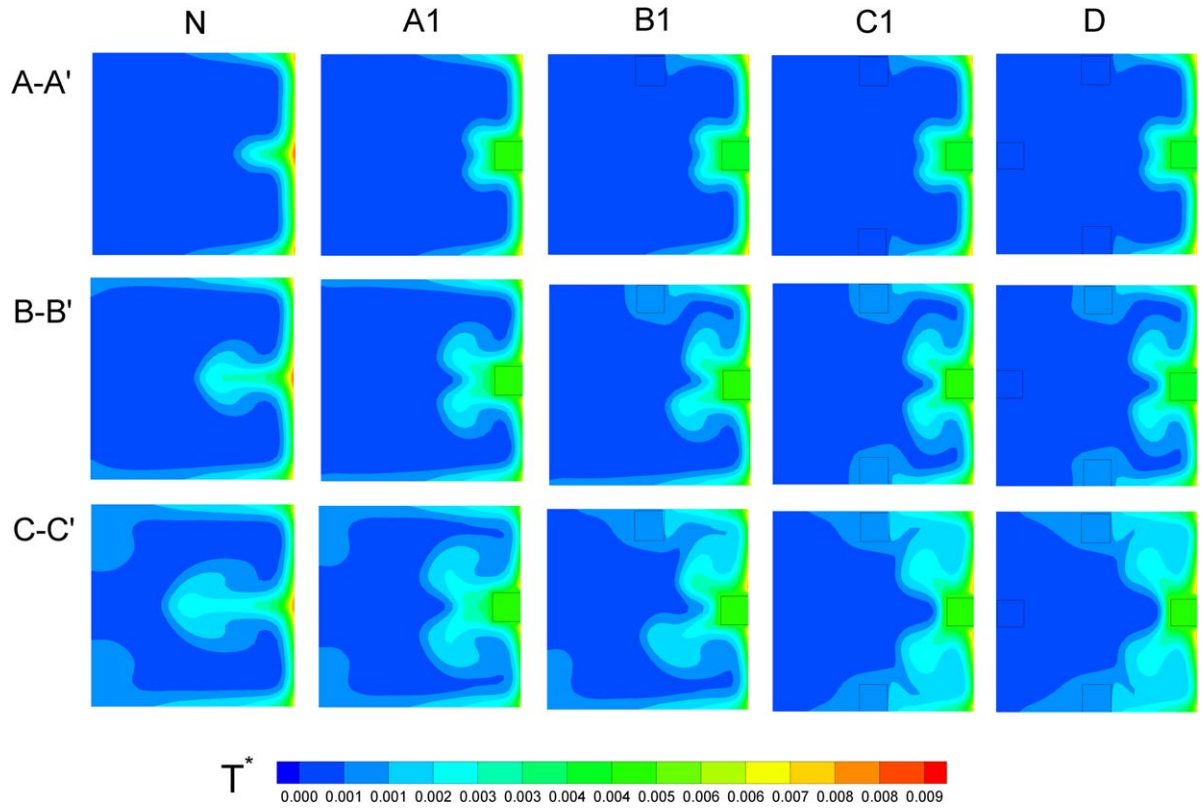

Fig. 6. Flow analysis: temperature contours on cross-sectional planes at A–A′, B–B′ and C–C′. (a) No rib, case N; (b) one rib, case A1; (c) two ribs, case B1; (d) three ribs, case C1; (e) four ribs, case D. On each cross-sectional plane, outer wall is at right-hand side, inner wall is at left-hand side.

cases is less than 10%. The largest value of T^* occurs in the non-rib case N, which confirms the addition of ribs is helpful for heat transfer enhancement. Among the five cases, the magnitude and the distribution of the temperature in cases C1 and D are the most similar, indicating once again that addition of rib on the inner wall has no significant influence on the flow field and heat transfer.

4.2. *Effects of rib number and arrangement on local distributions of entropy generation*

The distributions of entropy generations due to frictional irreversibility (S'''_P) and heat transfer irreversibility (S'''_T) on A–A′, B–B′ and C–C′ planes for the five cases are shown in Figs. 7 and 8, respectively. From Fig. 7, it can be seen that the significant S'''_P concentrates in the narrow region adjacent to the duct walls, which is resulted from the steepest velocity gradient in the near-wall regions. Notably, on all planes for the five cases, S'''_P is most insignificant on the inner-wall side, indicating least frictional irreversibility in the region near the inner wall. For all cases, the largest S'''_P appears in the region near the outer wall, and the largest value of S'''_P increases from A–A′ plane to C–C′ plane gradually as the flow develops along the duct. In addition, since the frictional irreversibility becomes more serious due to the increased solid surface from added ribs, the regions with significant S'''_P can be found to increase in the cases with more ribs. The distributions of S'''_T are shown in Fig. 8. From the figure, it is seen the major generation of S'''_T is concentrated in the vicinity of outer wall, where the external heat flux is applied. Among the five cases, the largest value of S'''_T occurs in the no-rib case, N, which indicates the ribs are helpful to reduce heat transfer irreversibility. For all cases, the largest value of S'''_T decreases as the flow develops from A–A′ plane to C–C′ plane. Comparing Figs. 7 and 8, it is noted that S'''_T is much larger than S'''_P. This indicates the entropy generation in the flow condition ($q^* = 0.112$, $De = 1000$) is dominated by heat transfer irreversibility. However, it is expected, that, as q^* decreases and De increases, S'''_T decreases while S'''_P increases. Fig. 9 shows the distribution of Be for the five cases. For all cases, the values of Be in the region adjacent to the outer wall are very close to one, which indicates the entropy generation in the region is dominated by the heat transfer irreversibility. From A–A′ plane to C–C′ plane, the region with Be greater than 0.5 becomes wider and extends from duct outer wall toward duct central zone gradually, which is the natural result of the heat transfer phenomena as the flow develops along downstream. The total entropy generation distribution for the five cases is shown in Fig. 10. Since the principal entropy generation comes from the heat transfer irreversibility, it can be seen that the distribution pattern of S'''_{gen} is very similar to that of S'''_T in which the significant S'''_{gen} is concentrated in the vicinity of the outer wall.

4.3. *Optimal analysis of cases with various De*

For optimal analysis, the resultant entropy generations in the whole duct flow are investigated. Figs. 11–14 show the val-

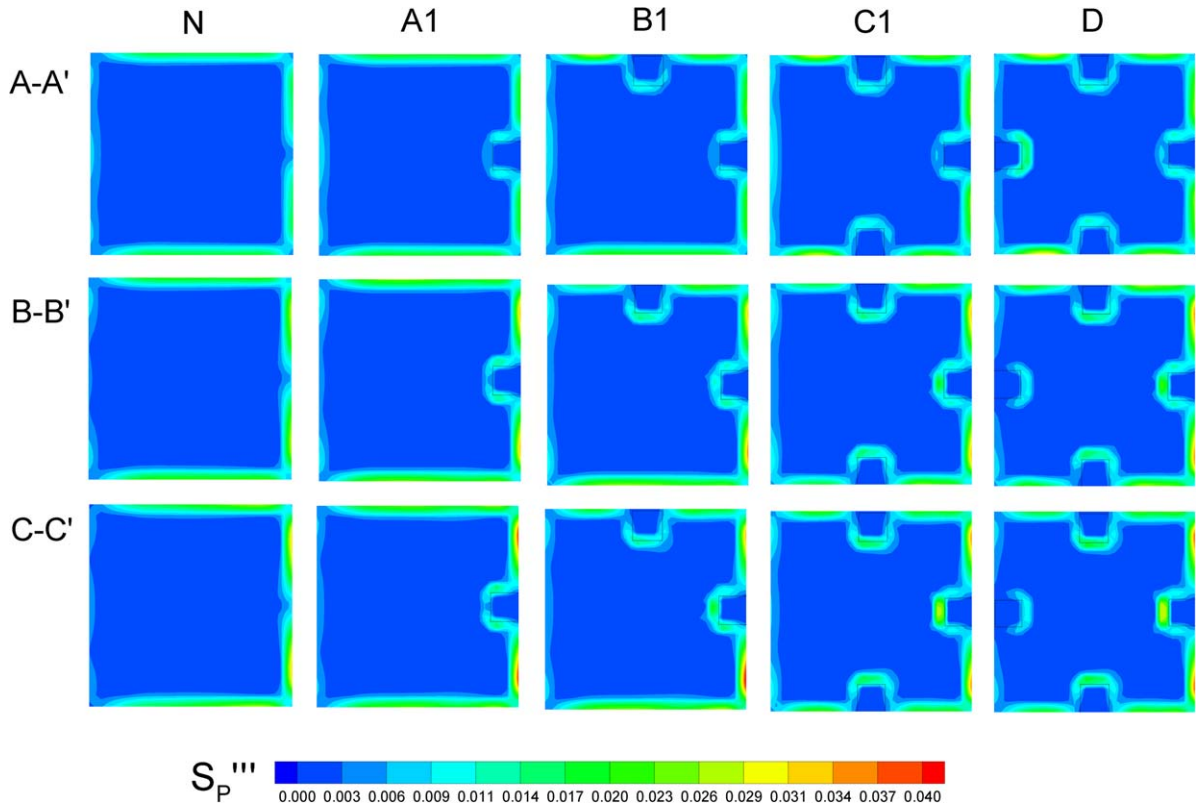

Fig. 7. The contours of volumetric entropy generation, S_P''' on cross-sectional planes at A–A′, B–B′ and C–C′. (a) No rib, case N; (b) one rib, case A1; (c) two ribs, case B1; (d) three ribs, case C1; (e) four ribs, case D. On each cross-sectional plane, outer wall is at right-hand side, inner wall is at left-hand side.

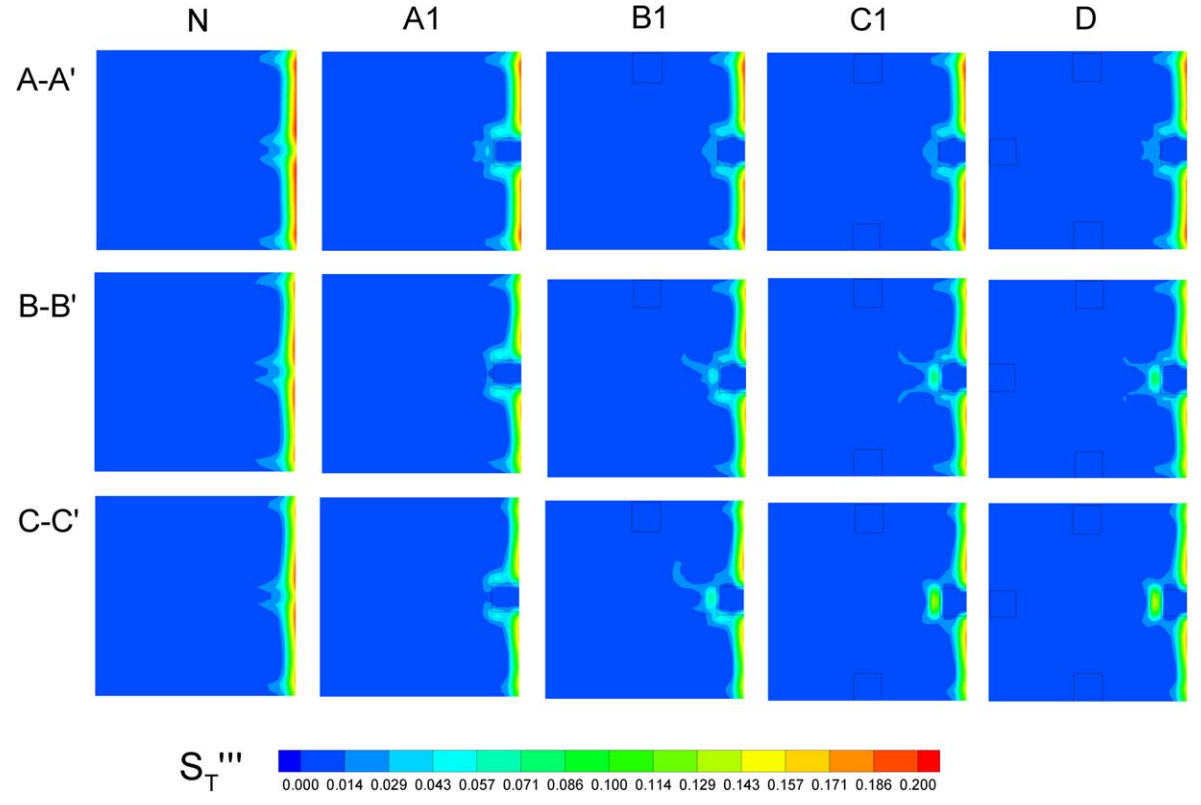

Fig. 8. The contours of volumetric entropy generation S_T''' on cross-sectional planes at A–A′, B–B′ and C–C′. (a) No rib, case N; (b) one rib, case A1; (c) two ribs, case B1; (d) three ribs, case C1; (e) four ribs, case D. Outer wall is at right-hand side, inner wall is at left-hand side.

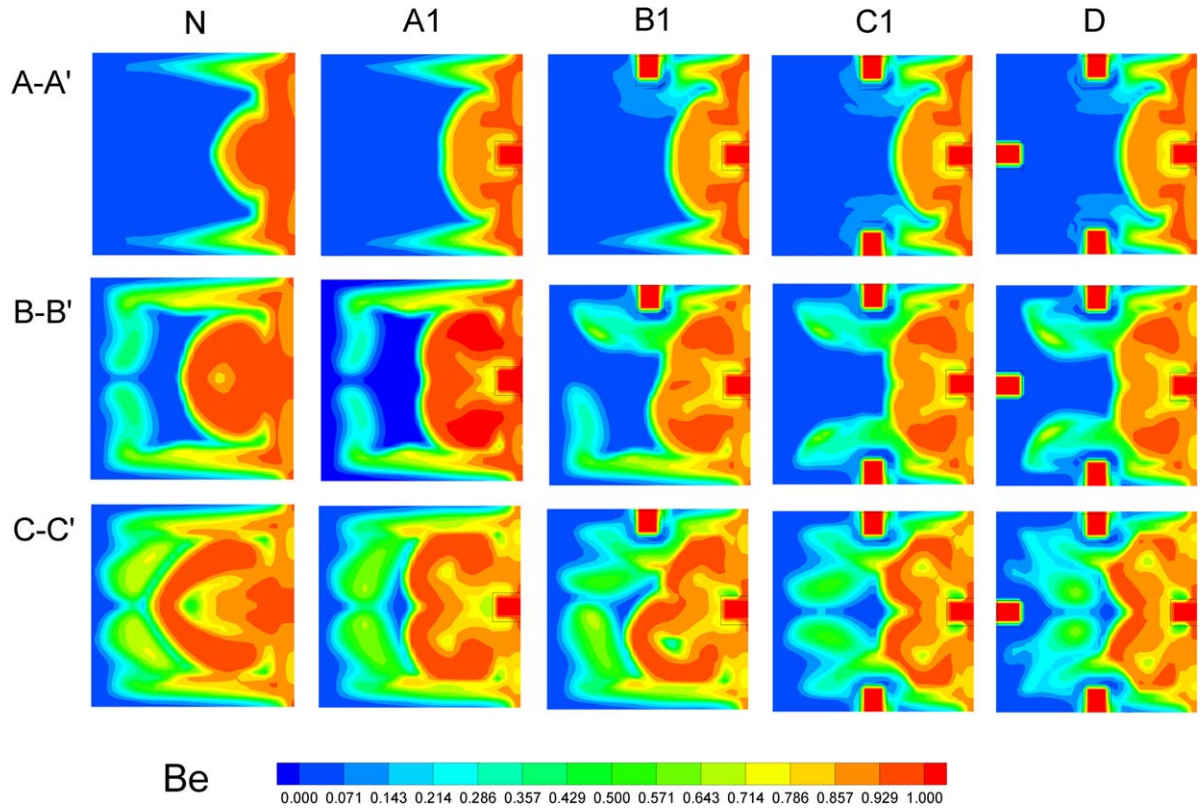

Fig. 9. The contours of *Be* on cross-sectional planes at A–A′, B–B′ and C–C′. (a) No rib, case N; (b) one rib, case A1; (c) two ribs, case B1; (d) three ribs, case C1; (e) four ribs, case D. On each cross-sectional plane, outer wall is at right-hand side, inner wall is at left-hand side.

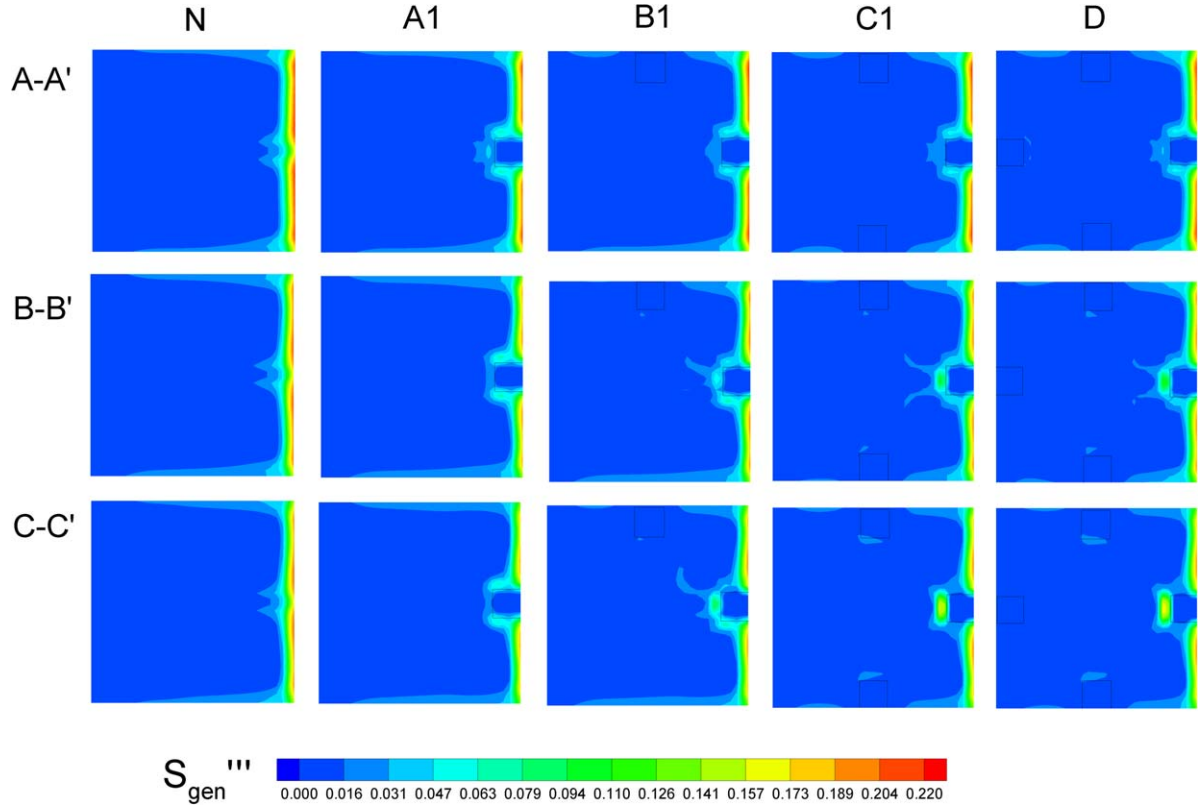

Fig. 10. The contours of volumetric entropy generation, S'''_{gen} on cross-sectional planes at A–A′, B–B′ and C–C′. (a) No rib, case N; (b) one rib, case A1; (c) two ribs, case B1; (d) three ribs, case C1; (e) four ribs, case D. On each cross-sectional plane, outer wall is at right-hand side, inner wall is at left-hand side.

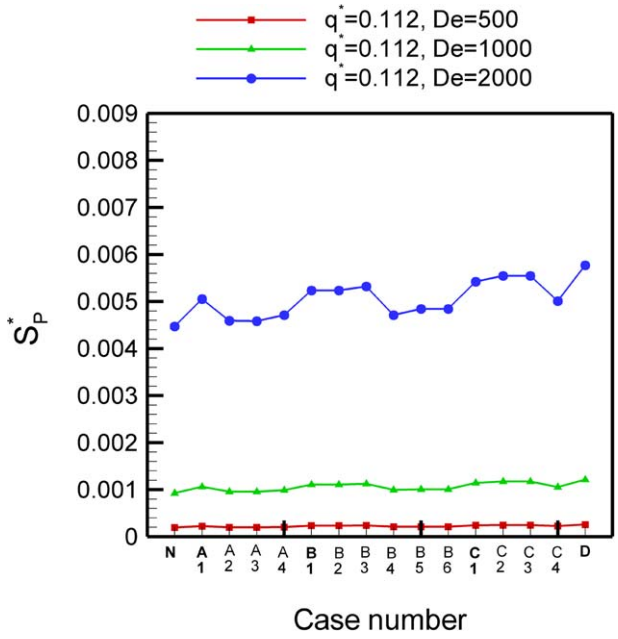

Fig. 11. S_P^* for all analyzed cases with various rib arrangements. $q^* = 0.112$ and $De = 500$, 1000, 2000.

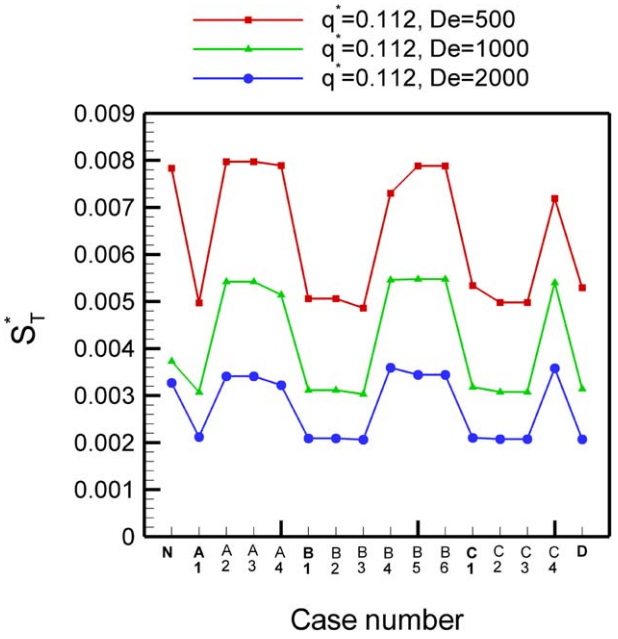

Fig. 12. S_T^* for all analyzed cases with various rib arrangements. $q^* = 0.112$ and $De = 500$, 1000, 2000.

ues of S_P^*, S_T^*, S_T^*/S_{gen}^* and S_{gen}^* for all cases studied. Three flow conditions: $q^* = 0.112$ with $De = 500$, 1000 and 2000, are included to investigate the De effects. Since the more serious frictional irreversibility is caused by larger-De flows, it is clearly seen from Fig. 11 that S_P^* is significantly raised as De increases. A general trend revealed from the figure indicates that the values of S_P^* in the group with more ribs are larger than those for group with less ribs. This comes from the natural result that more serious frictional irreversibility is produced due to increased solid interfaces with more ribs. In addition, a common feature can be found when comparing the values of S_P^* in each group, i.e. in the cases with rib mounted on outer wall (cases A1, B1, B2, B3, C1, C2, C3 and D), the values of S_P^* are raised most significantly. This result indicates the rib mounted on outer wall is very detrimental for the reduction of frictional irreversibility. Fig. 12 shows the values of S_T^* for all cases. Since the increase of De is helpful in enhancing heat transfer, the values of S_T^* become smaller for larger De. When comparing the cases in each group with different rib numbers, two important points are worth noting. First, not all added ribs can reduce the values of S_T^*. Only in cases with rib mounted on the outer wall (cases A1, B1, B2, B3 and C1, C2, C3 and D), significant reduction of S_T^* can be achieved. It is noted in the cases without rib mounted on the outer wall (cases A2, A3, A4, B4, B5, B6 and C4), the value of S_T^* remains as high level, or even becomes worse, when compared with the no-rib case. Second, in the ribbed cases with evident reduction of S_T^* (cases A1, B1, B2, B3 and C1, C2, C3 and D), the case with only one rib (case A1) exhibits good performance as that in cases with more added ribs (cases B1, B2, B3 and C1, C2, C3 and D). It is noted that the extra rib additions on other walls do not provide the further reduction of S_T^*. Fig. 13 shows the S_T^*/S_{gen}^* for all cases. From the figure, it is clearly found that the magnitude of S_T^*/S_{gen}^* becomes smaller for larger De. This is understood

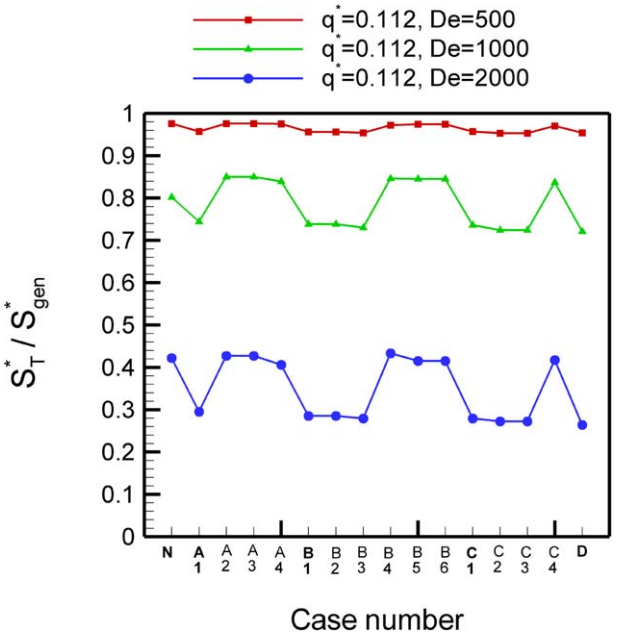

Fig. 13. S_T^*/S_{gen}^* for all analyzed cases with various rib arrangements. $q^* = 0.112$ and $De = 500$, 1000, 2000.

from the fact that the decrease in De will cause the decrease of S_P^* and the increase of S_T^*. Consequently, S_{gen}^* in smaller De cases will be dominated by heat transfer irreversibility with a relatively larger value of S_T^*/S_{gen}^*.

The above arguments demonstrate, regardless of the wall where ribs are, the addition of a rib causes the increase of S_P^*. But only in the cases with rib mounted on outer wall, S_T^* can be reduced significantly. The opposing influences of ribs on S_P^* and S_T^* require further investigation of final effects on resultant entropy generation, S_{gen}^*, for optimal analysis. The values of S_{gen}^* for all cases with various De are shown in Fig. 14. The op-

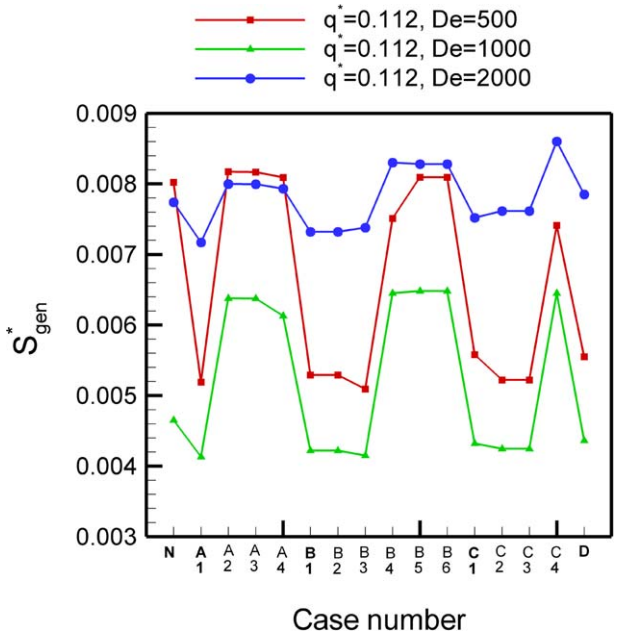

Fig. 14. S^*_{gen} for all analyzed cases with various rib arrangements. $q^* = 0.112$ and $De = 500$, 1000, 2000.

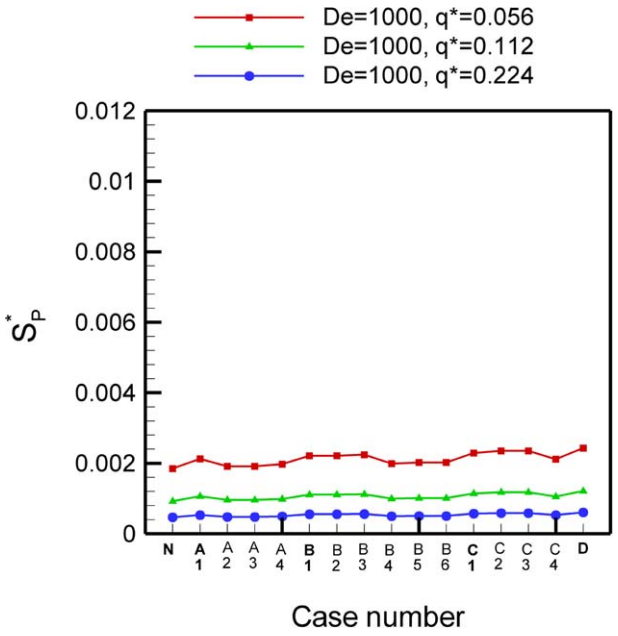

Fig. 15. S^*_P for all analyzed cases with various rib arrangements. $De = 1000$ and $q^* = 0.056$, 0.112 and 0.224.

posite influences of De on S^*_P and S^*_T induce a non-monotonic relation between De andS^*_{gen}. Comparing cases of various De, it is found that the cases with $De = 1000$ exhibit the optimal S^*_{gen} among the three cases. Besides, Fig. 14 also indicates a significant reduction of S^*_{gen} only appears in the cases with rib mounted on outer wall. For cases without rib mounted on outer wall (cases A2, A3, A4, B4, B5, B6 and C4), S^*_{gen} is not reduced, and even becomes worse than the no-rib case. When comparing the cases with rib mounted on outer wall (cases A1, B1, B2, B3 and C1, C2, C3 and D), the one-rib case (A1) shows good performance in S^*_{gen} reduction, whereas the addition of ribs on other wall cannot induce further reduction improvement in S^*_{gen}. Accordingly, it can be concluded that one-rib addition on the outer wall is the most effective way to reduce entropy generation in the flow field. Nonetheless, there is still one point worthy of special caution. Since the effects of rib on S^*_P and S^*_T are opposite when the rib is mounted on outer wall, the rib addition is more beneficial for those cases with S^*_T as the dominant source of entropy generation. It can be seen from Fig. 14 that the reduction of S^*_{gen} is the most effective for the cases with $De = 500$, which just reflects the above argument that the entropy generation in flow fields is more dominant by S^*_T for lower De and therefore the reduction of S^*_{gen} due to the heat transfer enhancement by the added ribs is more apparent in lower-De cases.

4.4. Optimal analysis of cases with various q^*

Figs. 15–18 show the values of S^*_P, S^*_T, S^*_T/S^*_{gen} and S^*_{gen} for cases with fixed De ($De = 1000$) and various heat flux ($q^* = 0.056$, 0.112 and 0.224), respectively, from which the effects of external heat flux are examined. Fig. 15 shows that the values of S^*_P are generally smaller in the larger-q^* cases. As pointed out in the previous study [19,20], since the temperature change in the flow fields is small, the influences of q^* on velocity distribution are very minor. Accordingly, no evident change of velocity gradients exists in the cases with various q^*. However, the values of denominators, T and $\dot{Q}$ appearing in the definition of S'''_P (Eq. (5)) and S^*_P (Eq. (9)), respectively, are larger in the cases with larger q^*, thus resulting the smaller S^*_P in the larger-q^* cases. The values of S^*_T for all cases are shown in Fig. 16. Because of the more significant transfer irreversibility caused by larger q^*, the values of S^*_T can be seen to increase with q^*. Similarly with previous discussions, only in the cases with rib mounted on outer wall (cases A1, B1, B2,

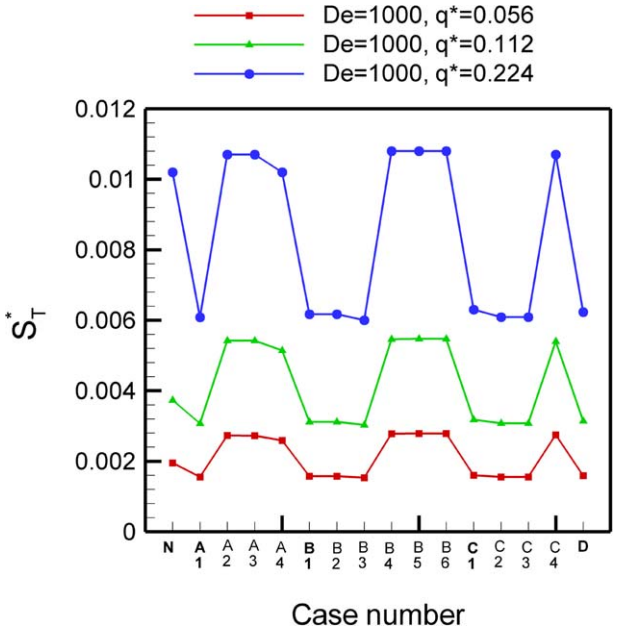

Fig. 16. S^*_T for all analyzed cases with various rib arrangements. $De = 1000$ and $q^* = 0.056$, 0.112, 0.224.

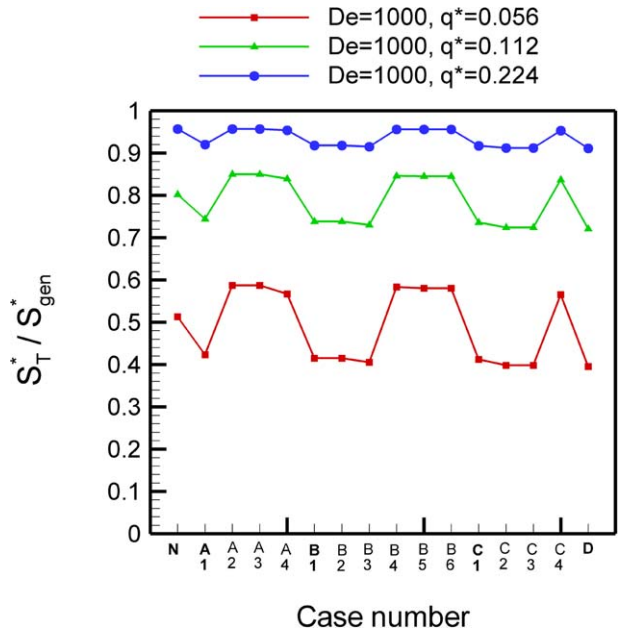

Fig. 17. S_T^*/S_{gen}^* for all analyzed cases with various rib arrangements. $De = 1000$ and $q^* = 0.056, 0.112, 0.224$.

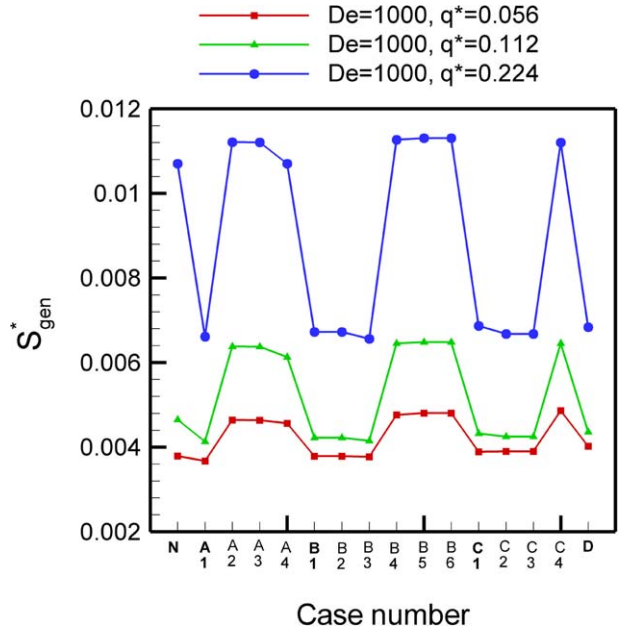

Fig. 18. S_{gen}^* for all analyzed cases with various rib arrangements. $De = 1000$ and $q^* = 0.056, 0.112, 0.224$.

B3 and C1, C2, C3 and D), S_T^* can be reduced. For other ribbed cases (cases A2, A3, A4, B4, B5, B6 and C4), the addition of ribs does not reduce S_T^*, but makes it worse. The increase of S_T^*/S_{gen}^* in the larger-q^* cases, as shown in Fig. 17, is resulted from two factors: the increase of S_T^* and decrease of S_P^* as q^* increases. For all cases with $q^* = 0.112$ and 0.224, and most of the cases with $q^* = 0.056$, the values of S_T^*/S_{gen}^* are larger than 0.5, which indicates the entropy generation in the flow fields with $De = 1000$ is dominated by heat transfer irreversibility in these cases. Fig. 18 shows the resultant entropy generation, S_{gen}^*, from which some results consistent with previous discussion can be observed. Apparently, S_{gen}^* becomes larger as q^* increases in the present flow conditions. For each group with specific q^*, only in the cases with rib mounted on outer wall (cases A1, B1, B2, B3 and C1, C2, C3 and D), S_{gen}^* can be effectively reduced. Besides, the reduction of S_{gen}^* is more evident in cases with larger q^*, in which the heat transfer irreversibility is more dominant in the flow field. For other ribbed cases (cases A2, A3, A4, B4, B5, B6 and C4), the addition of ribs does not reduce S_{gen}^*, but makes it worse. In all cases with rib mounted on outer wall (cases A1, B1, B2, B3 and C1, C2, C3 and D) for specific q^*, the amount of S_{gen}^* reduction is similar, indicating again that the case with one-rib mounted on outer wall is the optimal choice since the extra ribs mounted on other walls cannot provide further more S_{gen}^* reduction in the flow field.

5. Conclusions

The entropy generation and optimization for laminar forced convection in a rectangular curved duct with longitudinal ribs mounted on duct walls are investigated in the present study with numerical methods. The detailed information of local distributions of entropy generation due to frictional and heat transfer irreversibility as well as the overall entropy generation in the whole flow fields are analyzed separately. Through careful examination on the influences of various rib number and rib arrangement on entropy generations, several important conclusions are achieved that are summarized as follows.

(1) The flow fields in the curved duct, including the secondary flow motion, and the distributions of velocity and temperature, are all considerably influenced by the number and arrangement of mounted ribs.
(2) For all of the five selected baseline cases, including no-rib case N, one-rib case A1, two-rib case B1, three-rib case C1 and four-rib case D, S_P''' is significantly concentrated in the narrow region adjacent to the duct walls due to steep velocity gradient in the near-wall regions. Among the four sides of duct wall, the most significant S_P''' is distributed on the outer-wall side, whereas S_P''' is least at the inner-wall side. In the cases with more ribs, the additional solid surface increases frictional irreversibility, and accordingly cause the regions with significant generation of S_P''' to increase. The major generation of S_T''' concentrates in the vicinity of outer wall, where the external heat flux imposes. Among the five baseline cases, the largest value of S_T''' occurs in the none-rib case N, which indicates the added rib is helpful to reduce the heat transfer irreversibility. From the distributions of resultant entropy generation, S_{gen}''', it is also found the entropy in the flow field is principally generated in the vicinity of the outer wall for all cases.
(3) The overall entropy generation in the flow field due to frictional irreversibility, S_P^*, significantly increases with De and decreases for increasing q^*. The values of S_P^* for cases with more ribs are larger than those in the cases with less ribs, because of the more significant frictional irreversibility due to the increased solid faces. Particularly, in the cases with rib mounted on outer wall (cases A1, B1, B2, B3,

C1, C2, C3 and D), the values of S_P^* are apparently raised, indicating that the rib mounted on outer wall is the most detrimental for reduction in frictional irreversibility.

(4) The overall entropy generation in the flow field due to heat transfer irreversibility S_T^*, decreases with increasing De and increases as q^* increases. Only in cases with rib mounted on the outer wall (cases A1, B1, B2, B3 and C1, C2, C3 and D), the significant reduction of S_T^* can be achieved. For other cases with ribs mounted on other walls (cases A2, A3, A4, B4, B5, B6 and C4), the addition of ribs only induces very minor reduction in S_T^*, or even makes S_T^* worse than the no-rib case. Notably, in the cases with rib mounted on the outer wall, the case with only one rib (case A1) exhibits good performance as that in cases with more ribs added (cases B1, B2, B3 and C1, C2, C3 and D), which reveals that the extra rib additions on other walls do not provide further reduction of S_T^*.

(5) Regardless of the rib-mounted side-wall, ribs cause increase of S_P^*. But only in the cases with rib mounted on outer wall, S_T^*can be reduced significantly. Accordingly, the mounted rib is more beneficial for cases with S_T^* as the dominant source of entropy generation in the flow field. For such cases, one-rib addition on the outer wall is the most effective way to reduce the resultant entropy generation, S_{gen}^*, whereas the extra rib addition on other walls cannot give further evident improvement for S_{gen}^* reduction.

(6) The addition of rib on the heated wall can enhance the heat transfer performance, and in turn results the reduction in S_T^*.

References

[1] H. Ito, Flow in curved pipes, JMSE Int. J. 30 (1987) 543–552.

[2] Z.F. Dong, M.A. Ebadian, Numerical analysis of laminar flow in curved elliptic ducts, J. Fluid Eng. 113 (1991) 555–562.

[3] K.C. Cheng, J. Nakayama, M. Akiyama, Effect of finite and infinite aspect ratios on flow patterns in curved rectangular channels, in: Flow Visualisation, Tokyo, Japan, 1977, pp. 181–186.

[4] C.J. Bolinder, B. Sunden, Numerical prediction of laminar flow and forced convective heat transfer in a helical square duct with a finite pitch, Int. J. Heat Mass Transfer 39 (15) (1996) 3101–3115.

[5] L. Wang, Buoyancy-force-driven transition in flow structures and their effects on heat transfer in a rotating curved channel, Int. J. Heat Mass Transfer 40 (2) (1997) 220–235.

[6] R.J. Silva, R.M. Valle, M. Ziviani, Numerical hydrodynamic and thermal analysis of laminar flow in curved elliptic and rectangular ducts, International Journal of Thermal Sciences 38 (1999) 585–594.

[7] T.T. Chandratilleke, Secondary flow characteristics and convective heat transfer in a curved rectangular duct with external heating, in: Proc. of 5th World Conference on Experimental Heat Transfer, Fluid Mechanics and Thermodynamics [ExHFT-5], Thessaloniki, Greece, September 24–28, 2001.

[8] T.T. Chandratilleke, X. Nursubyakto, Numerical prediction of secondary flow and convective heat transfer in externally heated curved rectangular ducts, International Journal of Thermal Sciences 42 (2003) 187–198.

[9] C. Camci, D.H. Rizzo, Secondary flow and forced convection heat transfer near endwall boundary layer fences in a 90-deg turning duct, Int. J. Heat Mass Transfer 45 (2002) 831–843.

[10] A. Bejan, Entropy Generation Minimization, CRC Press, Boca Raton, FL, 1996.

[11] A. Bejan, Entropy Generation Through Heat and Fluid Flow, Wiley, New York, 1982.

[12] P.K. Nag, N. Kumar, Second law optimization of convection heat transfer through a duct with constant heat flux, Int. J. Energy Research 13 (1989) 537–543.

[13] A.Z. Sahin, Irreversibilities in various duct geometries with constant wall heat flux and laminar flow, Energy 23 (6) (1998) 465–473.

[14] A.Z. Sahin, Thermodynamics of laminar viscous flow through a duct subjected to constant heat flux, Energy 21 (12) (1996) 1179–1187.

[15] S.Z. Shuja, Optimal fin geometry based on exergoeconomic analysis for a pin-fin array with application to electronics cooling, Exergy 2 (2002) 248–258.

[16] O.N. Sara, S. Yapici, M. Yilmaz, T. Pekdemir, Secondary law analysis of rectangular channels with square pin-fins, Int. Comm. Heat Mass Transfer 28 (5) (2001) 617–630.

[17] T.H. Ko, K. Ting, Entropy generation and thermodynamic optimization of fully developed laminar convection in a helical coil, Int. Comm. Heat Mass Transfer 32 (2005) 214–223.

[18] T.H. Ko, Analysis of optimal Reynolds number for developing laminar forced convection in double-sine ducts based on entropy generation minimization principle, Energy Conversion and Management 47 (2006) 655–670.

[19] T.H. Ko, K. Ting, Entropy generation and optimal analysis for laminar forced convection in curved rectangular ducts: A numerical study, International Journal of Thermal Sciences 45 (2) (2006) 138–150.

[20] T.H. Ko, Numerical investigation on laminar forced convection and entropy generation in a curved rectangular duct with longitudinal ribs mounted on heated wall, International Journal of Thermal Sciences 45 (4) (2006) 390–404.

[21] T.H. Ko, K. Ting, Optimal Reynolds number for the fully developed laminar forced convection in a helical coiled tube, Energy: An International Journal, in press.

[22] T.H. Ko, Thermodynamic analysis of optimal curvature ratio for fully developed laminar forced convection in a helical coiled tube with uniform heat flux, International Journal of Thermal Sciences, in press.

[23] T.H. Ko, Numerical investigation on laminar forced convection and entropy generation in a helical coil with constant wall heat flux, Numerical Heat Transfer, Part A 49 (3) (2006) 257–278.

[24] T.H. Ko, Numerical analysis of entropy generation and optimal Reynolds number for developing laminar forced convection in double-sine ducts with various aspect ratios, International Journal of Mass and Heat Transfer 49 (3–4) (2006) 718–726.

[25] S. Paoletti, F. Rispoli, E. Sciubba, Calculation of exergetic losses in compact heat exchanger passages, ASME AES 10 (1989) 21–29.

[26] S.V. Patankar, Numerical Heat Transfer and Fluid Flow, Hemisphere, Washington, DC, 1980.